Electronic Supplementary Material (ESI) for Journal of Materials Chemistry A.

Electronic Supplementary Information

Role of Substituents in Determining Redox Potential of Organic Electrode Materials in Li/Na Rechargeable Batteries: Electronic Effects *vs.* Li/Na–Substituent Interaction

1. Materials and methods

Materials Preparation. All the commercially available reagents were used without further purification unless otherwise stated. All the syringes, magnetic stirring bars, glassware, and needles were completely dried in a convection oven. Thin layer chromatography (TLC) with commercial TLC plates (silica gel 60 F254, Merck Co.) was used to monitor the reactions. ^{1}H and ^{13}C NMR spectra were obtained using a Bruker Avance 300 spectrometer. FTIR spectra of pellets made from the terephthalate powders and KBr powder were obtained using an FT/IR-4200 (Jasco Inc., Japan) with a resolution of 4 cm^{-1}.

Synthesis of disodium terephthalate (Na_2TP). Sodium hydroxide (1.81 g, 45.2 mmol) and water (5 mL) were added to an ethanol solution (50 mL) containing terephthalic acid (**1**, 3.00 g, 18.6 mmol). The reaction mixture was stirred and refluxed overnight at 90 °C. After the reaction, the mixture was hot filtered and washed with ethanol. The filtered powder was dried in vacuo at 150 °C overnight to afford 2.70 g of white product (yield = 71%). ^{1}H NMR (300

MHz, D_2O) δ [ppm]: 7.91 (s, 4H, –ArH). ^{13}C NMR (75 MHz, D_2O) δ [ppm]: 128.59, 138.59, 175.28.

Synthesis of disodium 2,5-dimethylterephthalate (Na_2DMTP). Sodium hydroxide (1.03 g, 27.8 mmol) and water (5 mL) were added to an ethanol solution (50 mL) containing 2,5-dimethylterephthalic acid (**2**, 2.00 g, 10.3 mmol). The reaction mixture was stirred and refluxed overnight at 90 °C. After the reaction, the mixture was hot filtered and washed with ethanol. The filtered powder was dried in vacuo at 150 °C overnight to afford 2.01 g of pale gray product (yield = 82%). ^{1}H NMR (300 MHz, D_2O) δ [ppm]: 7.44 (s, 2H, –ArH), 2.34 (s, 6H, $–CH_3$). ^{13}C NMR (75 MHz, D_2O) δ [ppm]: 18.53, 127.81, 131.03, 139.54, 178.85.

Synthesis of diethyl 2,5-dimethoxyterephthalate (4). Potassium carbonate (6.52 g, 47.2 mmol) and methyl iodide (2.94 mL, 47.2 mmol) were added to *N,N*-dimethylformamide (DMF) solution (50 mL) containing diethyl 2,5-dihydroxyterephthalate (**3**, 2.00 g, 7.87 mmol). The reaction mixture was stirred and refluxed overnight at 40 °C. The cooled crude mixture was poured into water and titrated to pH 7 using 1.0 M hydrochloric acid. The precipitate was filtered and dried in vacuo at room temperature overnight to afford 2.10 g of powder (yield = 95%). ^{1}H NMR (300 MHz, $CDCl_3$) δ [ppm]: 7.37 (s, 2H, –ArH), 4.39 (q, *J* = 7.1 Hz, 4H, $–CH_2–$), 3.89 (s, 6H, $–OCH_3$), 1.40 (t, *J* = 7.1 Hz, 6H, $–CH_3$).

Synthesis of 2,5-dimethoxyterephthalic acid (5). Sodium hydroxide (1.79 g, 44.6 mmol) was added to an ethanol solution (50 mL) containing diethyl 2,5-dimethoxyterephthate (**4**, 2.10 g, 7.44 mmol). The reaction mixture was stirred and refluxed overnight at 90 °C. The cooled crude mixture was poured into water and titrated to pH 4 using 1.0 M hydrochloric acid. The precipitate was filtered and dried in vacuo at room temperature overnight to afford 1.70 g of powder (yield = 100%). ^{1}H NMR (300 MHz, DMSO-d$_6$) δ [ppm]: 13.0 (s, 2H, –COOH), 7.30 (s, 2H, –ArH), 3.79 (s, 6H, –OCH$_3$).

Synthesis of disodium 2,5-dimethoxyterephthalate (Na_2MeO_2TP). Sodium hydroxide (0.75 g, 18.8 mmol) and water (5 mL) were added to an ethanol solution (50 mL) containing 2,5-dimethoxyterephthalic acid (**5**, 1.70 g, 7.52 mmol). The reaction mixture was stirred and refluxed overnight at 90 °C. After the reaction, the mixture was hot filtered and washed with ethanol. The filtered powder was dried in vacuo at 150 °C overnight to afford 1.80 g of white product (yield = 89%). ^{1}H NMR (300 MHz, D_2O) δ [ppm]: 7.11 (s, 2H, –ArH), 3.84 (s, 6H, –OCH$_3$). ^{13}C NMR (75 MHz, D_2O) δ [ppm]: 56.37, 112.62, 129.67, 149.46, 175.36.

Electrochemical measurements. The Li and Na metal anodes were prepared in an Ar-filled glove box. The cathodes were fabricated by mixing 40% w/w active materials, 40% w/w carbon black (Super P), and 20% w/w PTFE (Aldrich) binder. A porous glass microfiber membrane (GF/F; Whatman, UK) was used as a separator in both the Li-and Na-ion cells. In the Li-ion cell, 1 M $LiPF_6$ in ethylene carbonate (EC)/dimethyl carbonate (DMC) (1:1 v/v, Techno Semichem Co., Ltd., Korea) was used as the electrolyte, and in the Na-ion cell, 1 M $NaClO_4$ in EC/DMC (1:1 v/v, Techno Semichem Co., Ltd., Korea) was used as the electrolyte. The cells were assembled in an inert atmosphere within an Ar-filled glove box. The discharge and charge measurements were performed at a constant current density of 40 mA g^{-1} in the voltage ranges of 0.5–3.0 V in the Li-ion cell and 0.2–2.7 V in the Na-ion cell using a battery test system (Won-A Tech, Korea).

Computational details. DFT calculations were performed using the Gaussian 09 quantum-chemical package.[S1] The geometries of all the Na_2TPs and anions were fully optimized in the gas phase using the B3LYP functional and 6-311G+(d,p) basis set. Vibrational frequency calculations were performed for the obtained structures at the same level to confirm the stable minima and examine thermochemical data.

The electron affinity (EA) values of the Na_2TPs were determined using $E_{(Na2TP)} - E_{(anion)}$, where $E_{(Na2TP)}$ and $E_{(anion)}$ denote the sum of the electronic and zero-point energies for the Na_2TPs and the corresponding anions, respectively.

The lithiated and sodiated Na_2TPs were constructed by adding either Li or Na atoms to the corresponding optimized dianions, respectively. Further geometry optimization processes for the neutral Na_2TPs, corresponding dianions, and lithiated and sodiated ones were performed in the solvated state at the same level. The effect of the solvent was considered by using the polarizable continuum model with the static and optical dielectric constant (ε = 46.4335, ε_{inf} = 1.942) for the electrolyte used in the experiment (EC:DMC = 1:1 v/v; ε_{EC} = 89.78, $\varepsilon_{inf,EC}$ = 2.014, ε_{DMC} = 3.087, $\varepsilon_{inf,DMC}$ = 1.87). Vibrational frequency calculations were also performed for the obtained structures in the solvated state at the same level to confirm the stable minima and examine the thermochemical data. We performed a search for the lowest-energy geometry by placing the Li and Na ions in different initial positions of the Na_2TPs followed by relaxation.

The redox potential of the reduction was calculated using the formula:

$$E_{red} = -\left(G_{dianion} - G_{Na2TP}\right) / nF, \qquad (1)$$

where G_{Na2TP} and $G_{dianion}$ are the Gibbs free energy of the Na_2TPs and of the corresponding dianions formed by the two-electron reduction in the solvated state, respectively; n is the number of electrons involved in the reduction; and F is the Faraday constant (see Figure S3a for the redox reaction schemes).

For the reference potentials, the potentials of Li/Li^+ and Na/Na^+ were calculated to be 0.92 and 1.36 V *vs.* vacuum, respectively, using the following formula (2):

$$E_{red} = -(G_M - G_{M^+}) / nF, \tag{2}$$

where G_M and G_{M^+} are the Gibbs free energy of the metal atom and corresponding cation, respectively.

The redox potentials of the lithiation and sodiation reactions were calculated using the formula

$$E_{red} = -(G_{\text{lithiated (or sodiated) form}} - G_{Na2TP} - 2G_{\text{Li (or Na)}}) / nF, \tag{3}$$

where G_{Na2TP}, $G_{\text{lithiated (or sodiated) form}}$, and $G_{\text{Li (or Na)}}$ are the Gibbs free energy of the NaTPs, the corresponding lithiated or sodiated forms, and either a Li or Na atom in the solvated state, respectively (see Figure S3b for the lithiation or sodiation schemes).

2. Supplementary tables

Table S1 | Electron Affinities (EA) of Na_2TPs.

	Neutral	**Anion**	**Electron Affinity**	
			in hartrees	in eV
Na_2TP	-932.998068	-933.030224	0.032156	**0.875009259**
Na_2DMTP	-1011.588108	-1011.619945	0.031837	**0.866328828**
Na_2MeO_2TP	-1162.02403	-1162.054479	0.030449	**0.828559427**

Table S2 | Redox Potentials of Metal Ions.

	Cation (hartree)	**Neutral Atom (hartree)**	**Redox Potential (V *vs.* vacuum)**
Na	-162.260004	-162.310131	**1.364057552**
Li	-7.489763	-7.523534	**0.918977549**

Table S3 | Reduction Potentials of Na_2TPs.

	Neutral (hartree)	**Dianion (hartree)**	**Reduction Potential**	
			V *vs.* Na/Na^+	V *vs.* Li/Li^+
Na2TP	-933.137762	-933.252764	**0.200661528**	**0.645741531**
Na2DMTP	-1011.730302	-1011.831511	**0.012993746**	**0.458073749**
Na2MeO2TP	-1162.180301	-1162.286472	**0.080506798**	**0.525586801**

Table S4 | Reduction Potentials of Na_2TPs with Consideration of Di-Sodium Insertion.

	Neutral (hartree)	**Sodiated (hartree)**	**Reduction Potential**	**Na-binding Energy**
			V *vs.* Na/Na^+	eV
Na2TP	-933.137762	-1257.788259	**0.411377901**	0.21072
Na2DMTP	-1011.730302	-1336.37146	**0.284311315**	0.27132
Na2MeO2TP	-1162.180301	-1486.838162	**0.511572605**	0.43107

Table S5 | Reduction Potentials of Na_2TPs with Consideration of Di-Lithium Insertion.

	Neutral (hartree)	**Lithiated (hartree)**	**Reduction Potential**	**Li-binding Energy**
			V *vs.* Li/Li^+	eV
Na2TP	-933.137762	-948.264247	**1.080548992**	0.43481
Na2DMTP	-1011.730302	-1026.845411	**0.925766951**	0.46769
Na2MeO2TP	-1162.180301	-1177.324657	**1.323702108**	0.79812

3. Supplementary figures

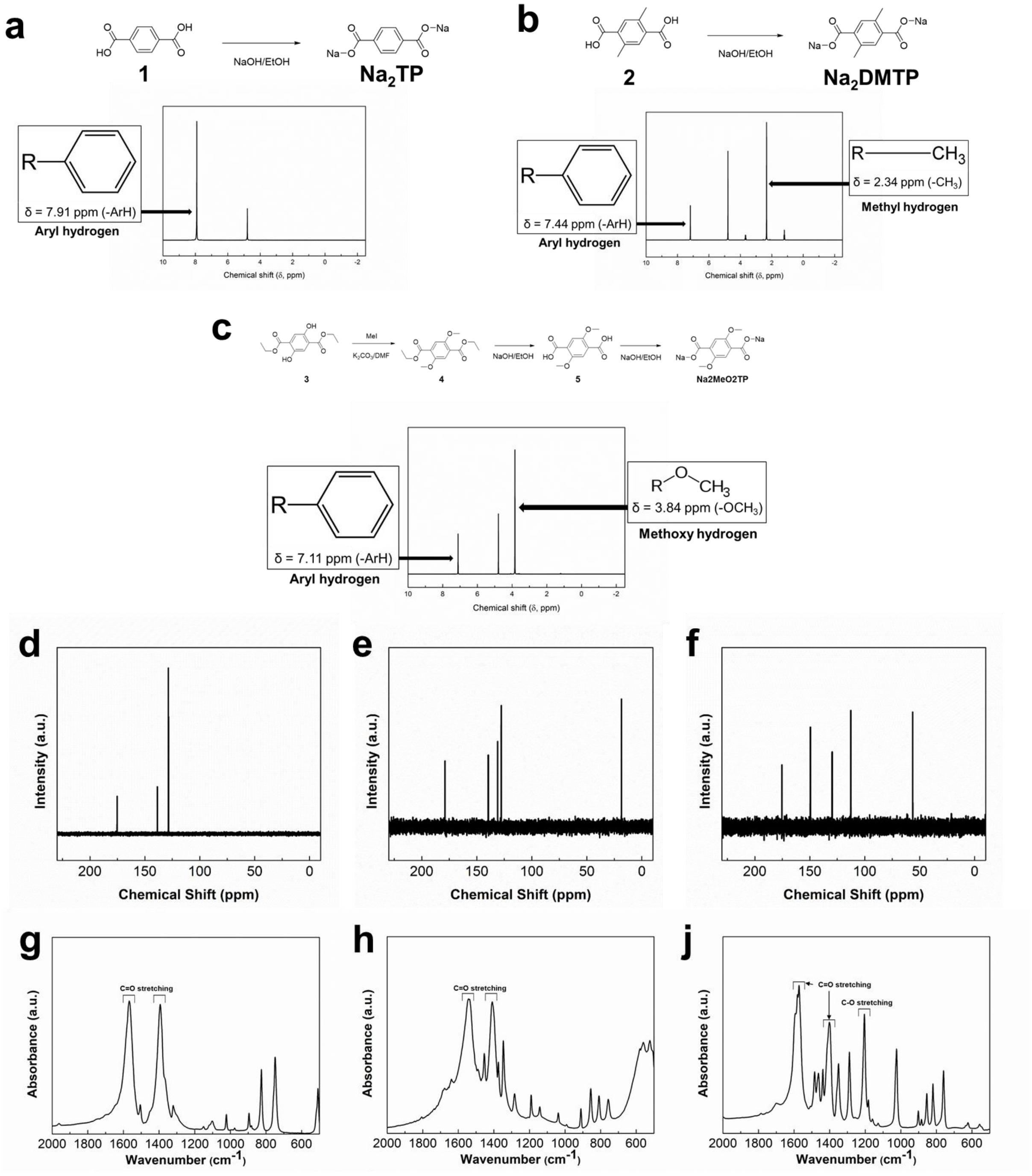

Figure S1 | Material characterization of synthesized terephthalates series. ^{1}H NMR data of (**a**) disodium terephthalate (Na_2TP), (**b**) disodium dimethylterephthalate (Na_2DMTP), and (**c**) disodium dimethoxyterephthalates (Na_2MeO_2TP). ^{13}C NMR data of (**d**) disodium terephthalate (Na_2TP), (**e**) disodium dimethylterephthalate (Na_2DMTP), and (**f**) disodium dimethoxyterephthalate (Na_2MeO_2TP). FT-IR data of (**g**) disodium terephthalate (Na_2TP), (**h**) disodium dimethylterephthalate (Na_2DMTP), and (**j**) disodium dimethoxyterephthalate (Na_2MeO_2TP).

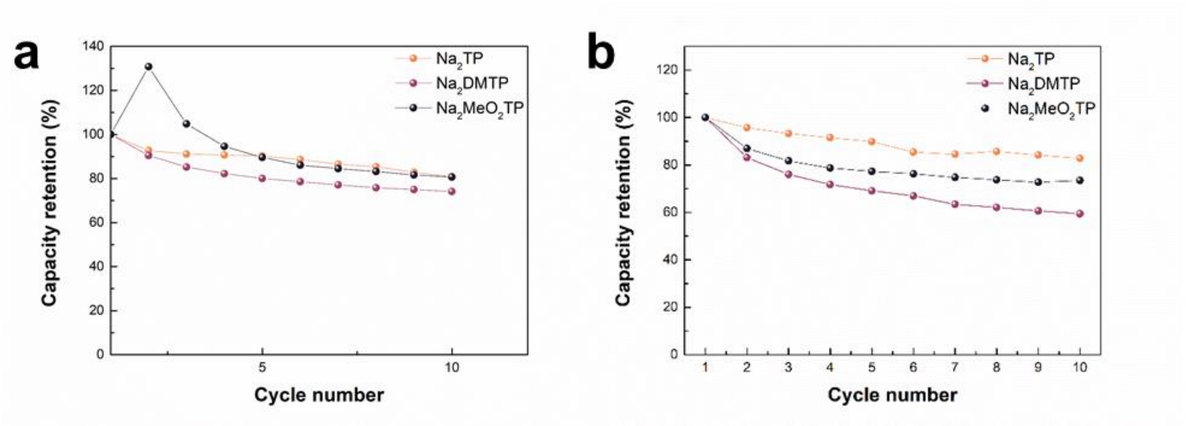

Figure S2 | Cycle stability of the terephthalate anodes. Capacity retention curve of the terephthalate anodes in (**a**) Na and (**b**) Li cells, respectively.

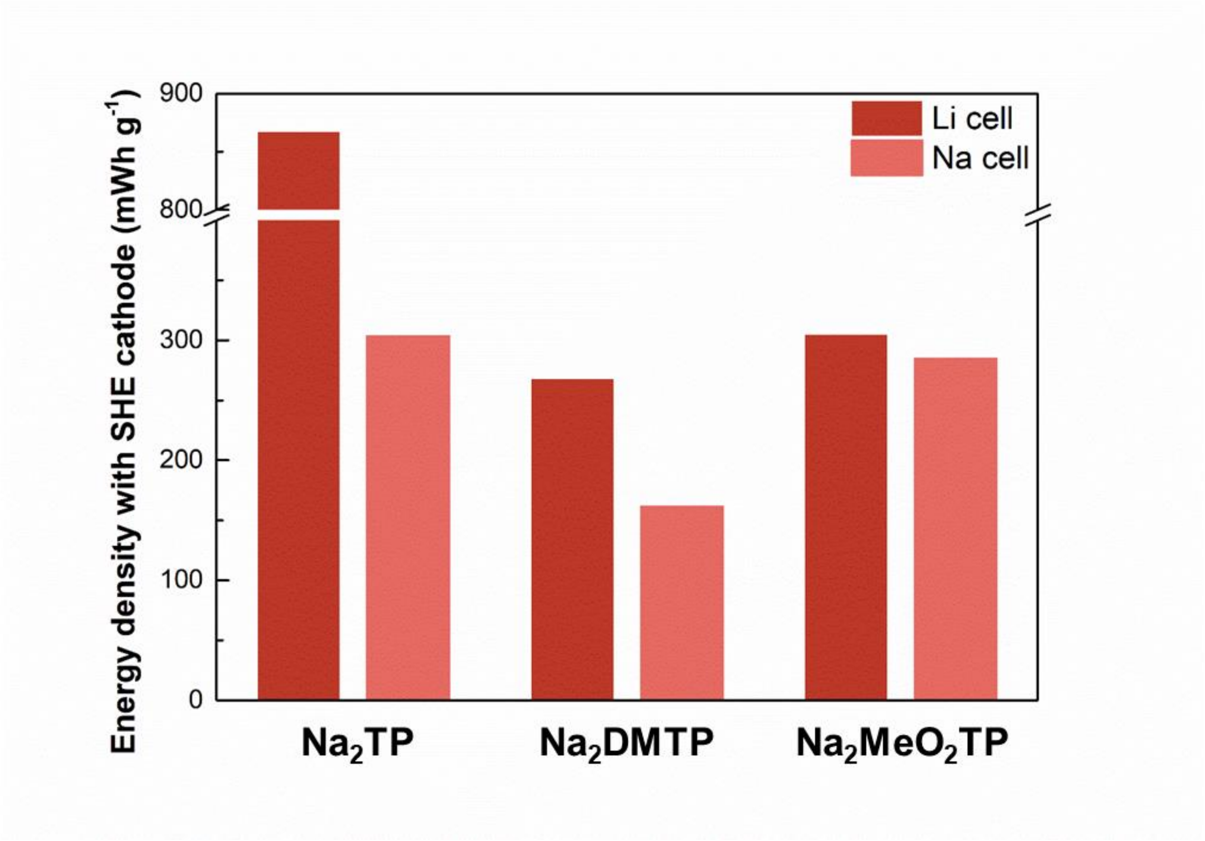

Figure S3 | Energy density comparison of the terephthalate anodes. Energy density with SHE hypothetical cathode of Na_2TP derivatives.

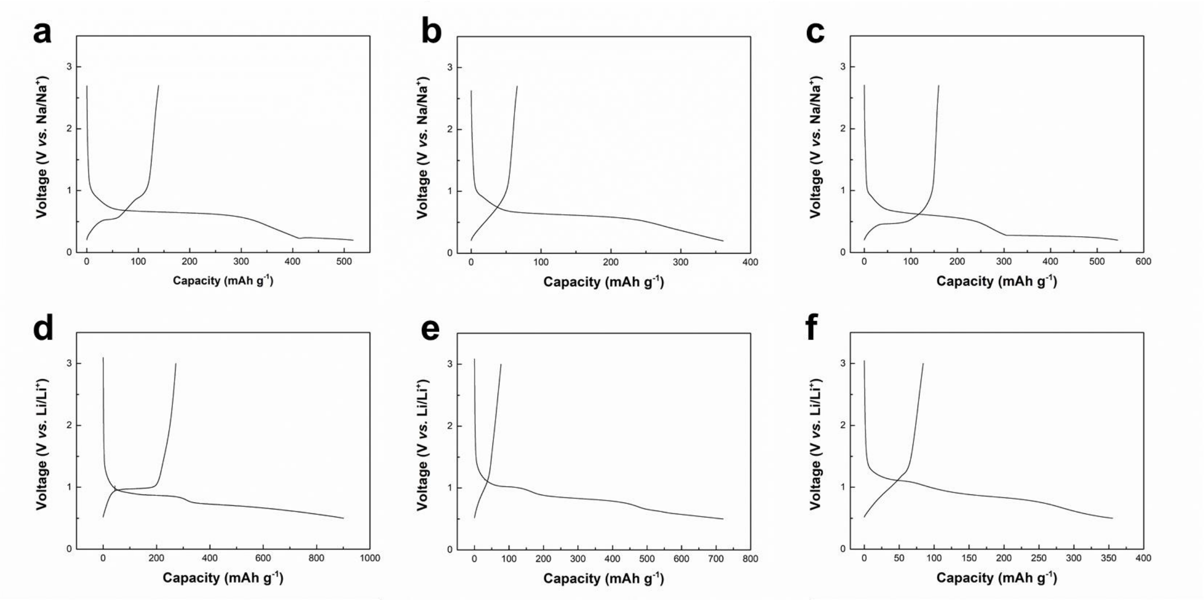

Figure S4 | Voltage profiles of Na_2TPs at the 1st cycle Capacity–voltage profiles of (**a, d**) disodium terephthalate (Na_2TP), (**b, e**) disodium dimethylterephthalate (Na_2DMTP), and (**c, f**) disodium dimethoxyterephthalate (Na_2MeO_2TP) in Na and Li cells, respectively.

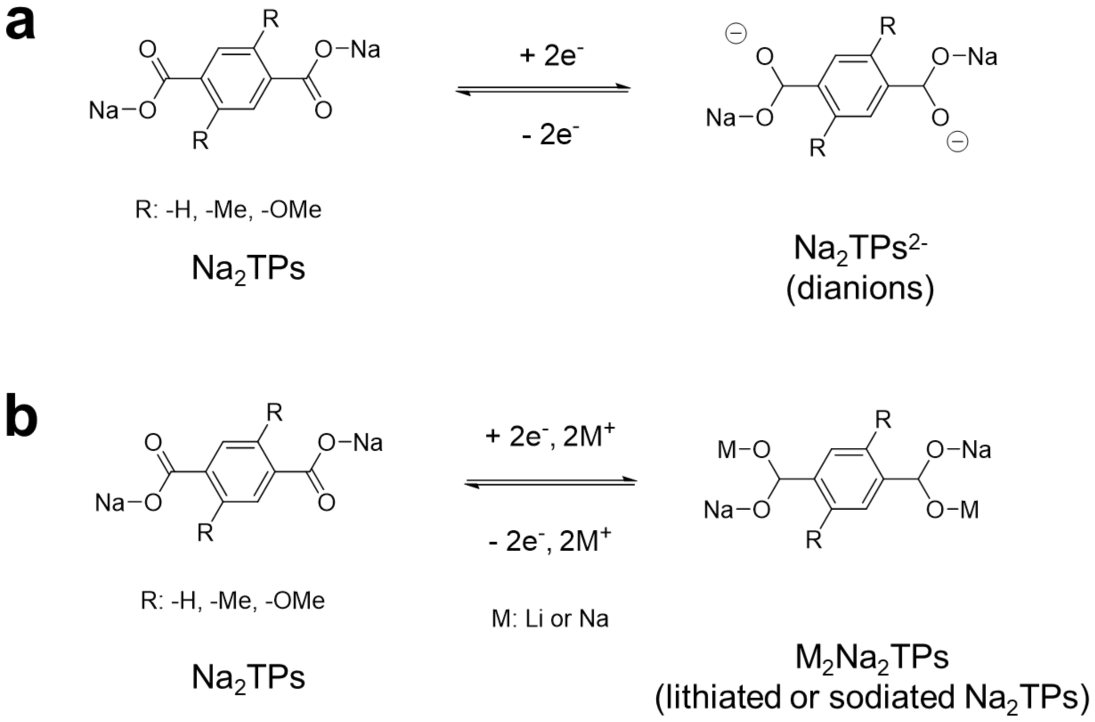

Figure S5 | Redox reaction schemes of Na_2TPs. Suggested redox reaction schemes of Na2TPs considering (**a**) with and (**b**) without charge carrying ions.

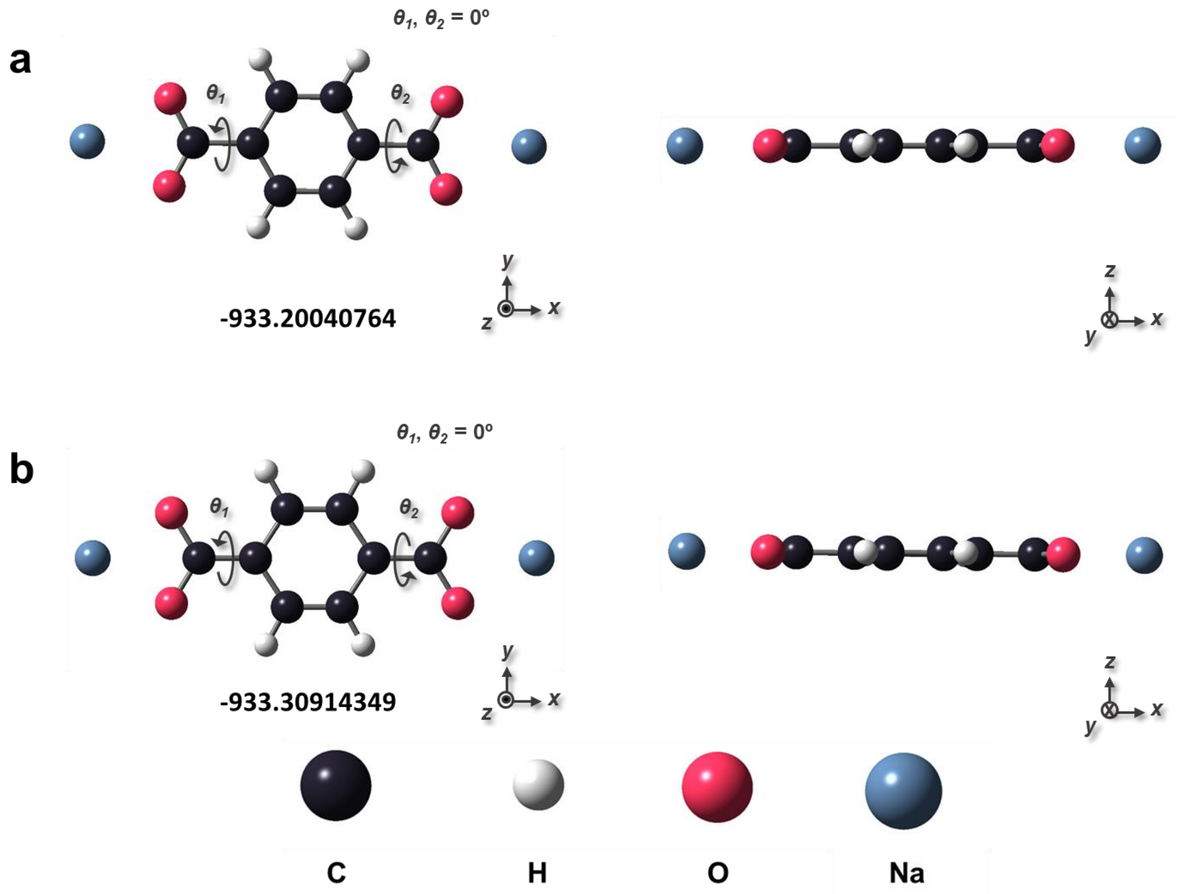

Figure S6 | Optimized geometries and total energy (in hartrees) of Na_2TP in solvated state. (**a**) Na_2TP and (**b**) Na_2TP^{2-}**.** Top views and side views are represented in the left and right panels along the Cartesian axes, respectively.

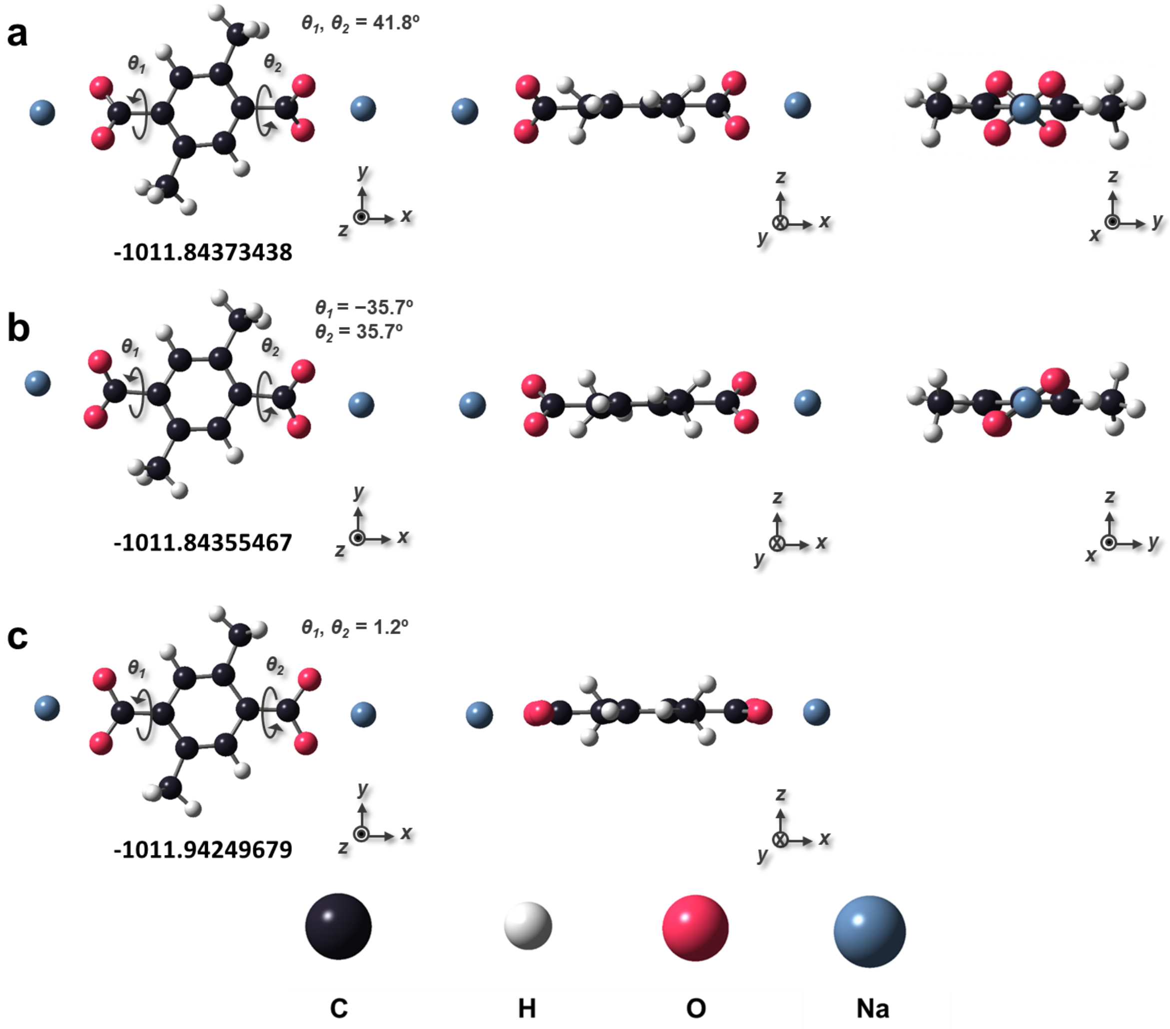

Figure S7 | Optimized geometries and total energy (in hartrees) of Na$_2$DMTP in solvated state. (**a**, **b**) Different conformations of Na$_2$DMTP and (**c**) Na$_2$DMTP^{2-}. Top views (left panels) and side views (middle and right panels) are represented along the Cartesian axes, respectively.

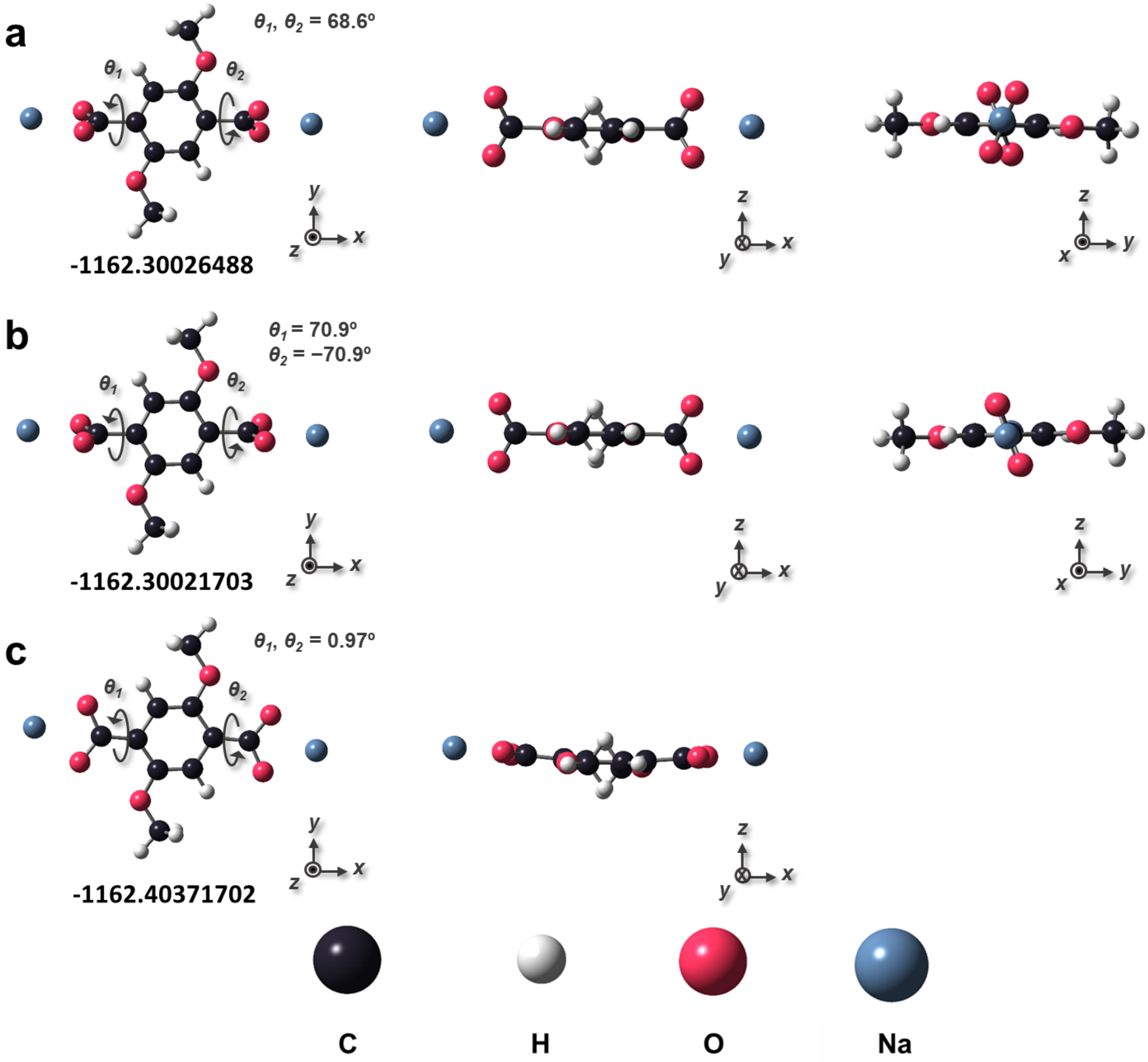

Figure S8 | Optimized geometries and total energy (in hartrees) of Na_2MeO_2TP in solvated state. (**a**, **b**) Different conformations of Na_2MeO_2TP and (**c**) $Na_2MeO_2TP^{2-}$**.** Top views (left panels) and side views (middle and right panels) are represented along the Cartesian axes, respectively.

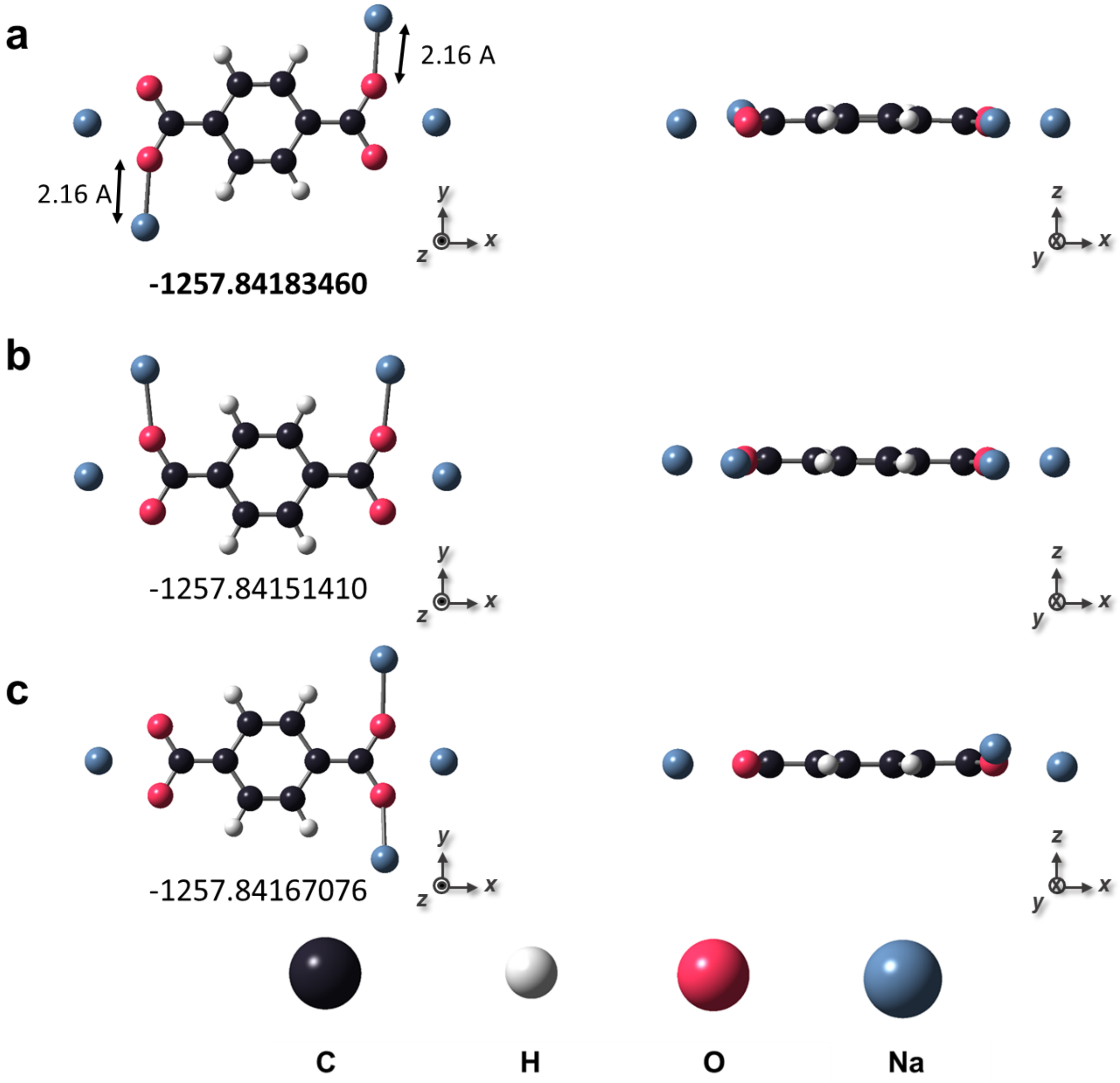

Figure S9 | Optimized geometries and total energy (in hartrees) of Na_2TP in solvated state after sodiation. (**a**) The most stable geometry and (**b**, **c**) different geometries of di-sodiated Na_2TP**.** Top views and side views are represented in the left and right panels along the Cartesian axes, respectively.

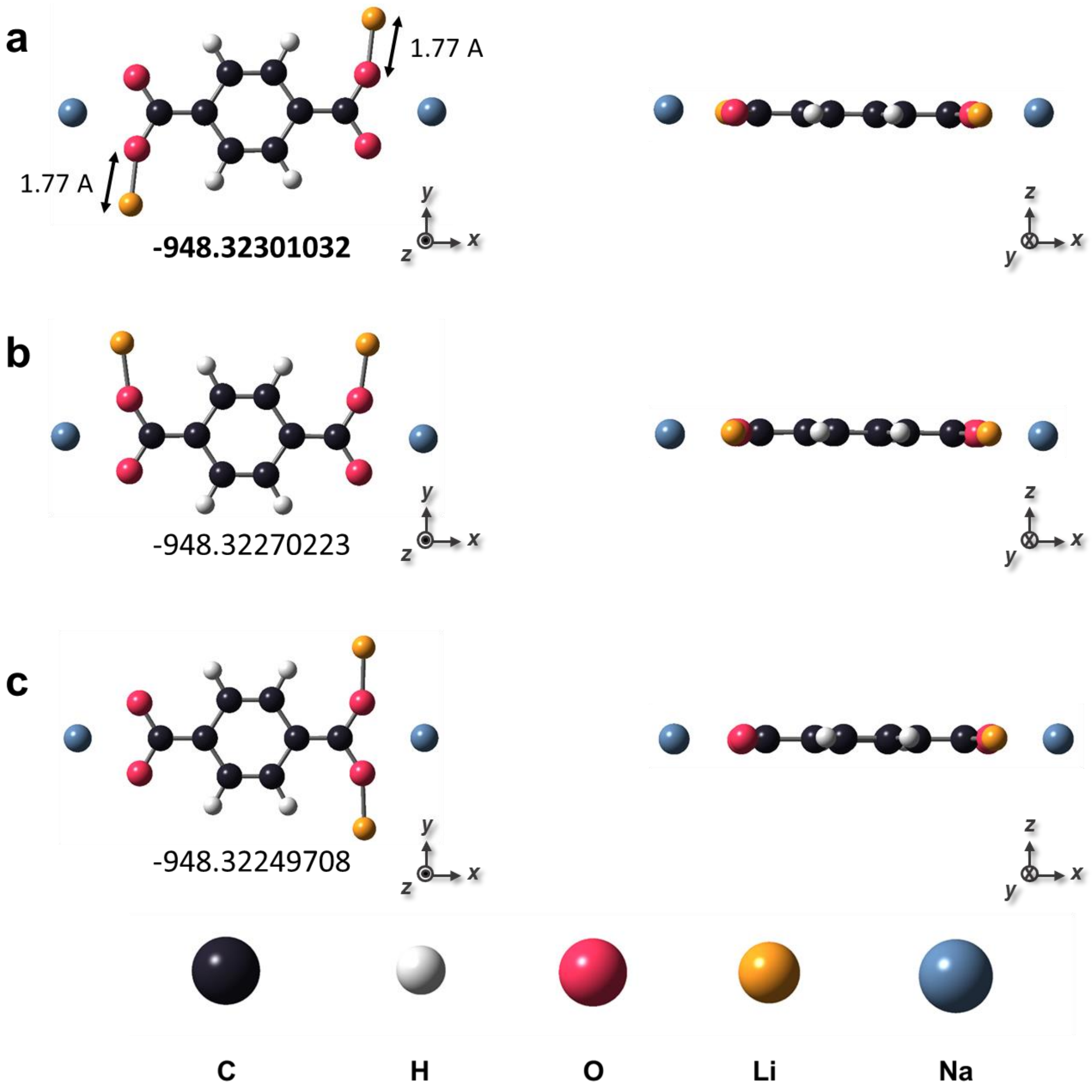

Figure S10 | Optimized geometries and total energy (in hartrees) of Na$_2$TP in solvated state after lithiation. (**a**) The most stable geometry and (**b**, **c**) different geometries of di-lithiated Na$_2$TP**.** Top views and side views are represented in the left and right panels along the Cartesian axes, respectively.

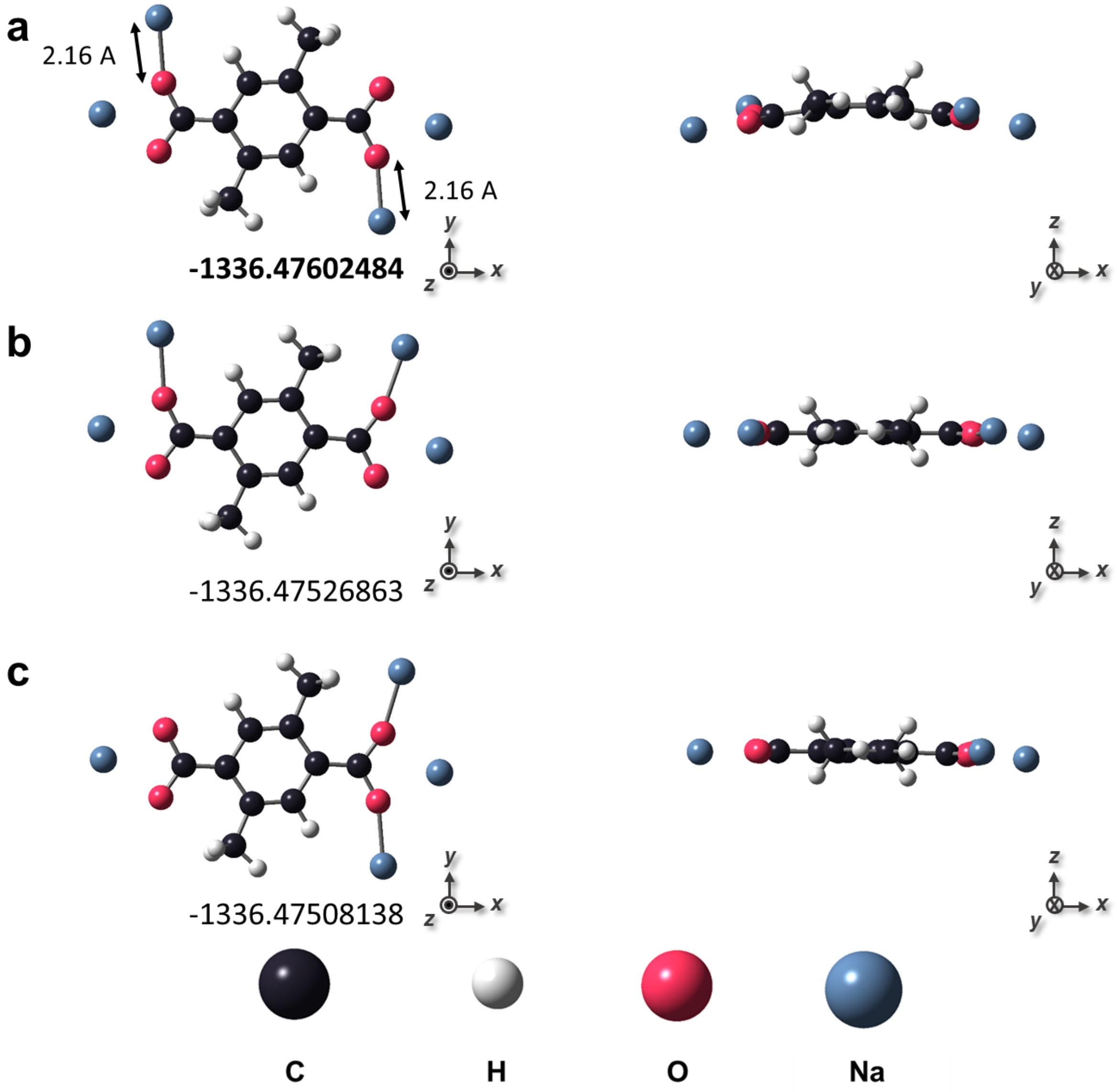

Figure S11 | Optimized geometries and total energy (in hartrees) of Na$_2$DMTP in solvated state after sodiation. (**a**) The most stable geometry and (**b**, **c**) different geometries of di-sodiated Na$_2$DMTP**.** Top views and side views are represented in the left and right panels along the Cartesian axes, respectively.

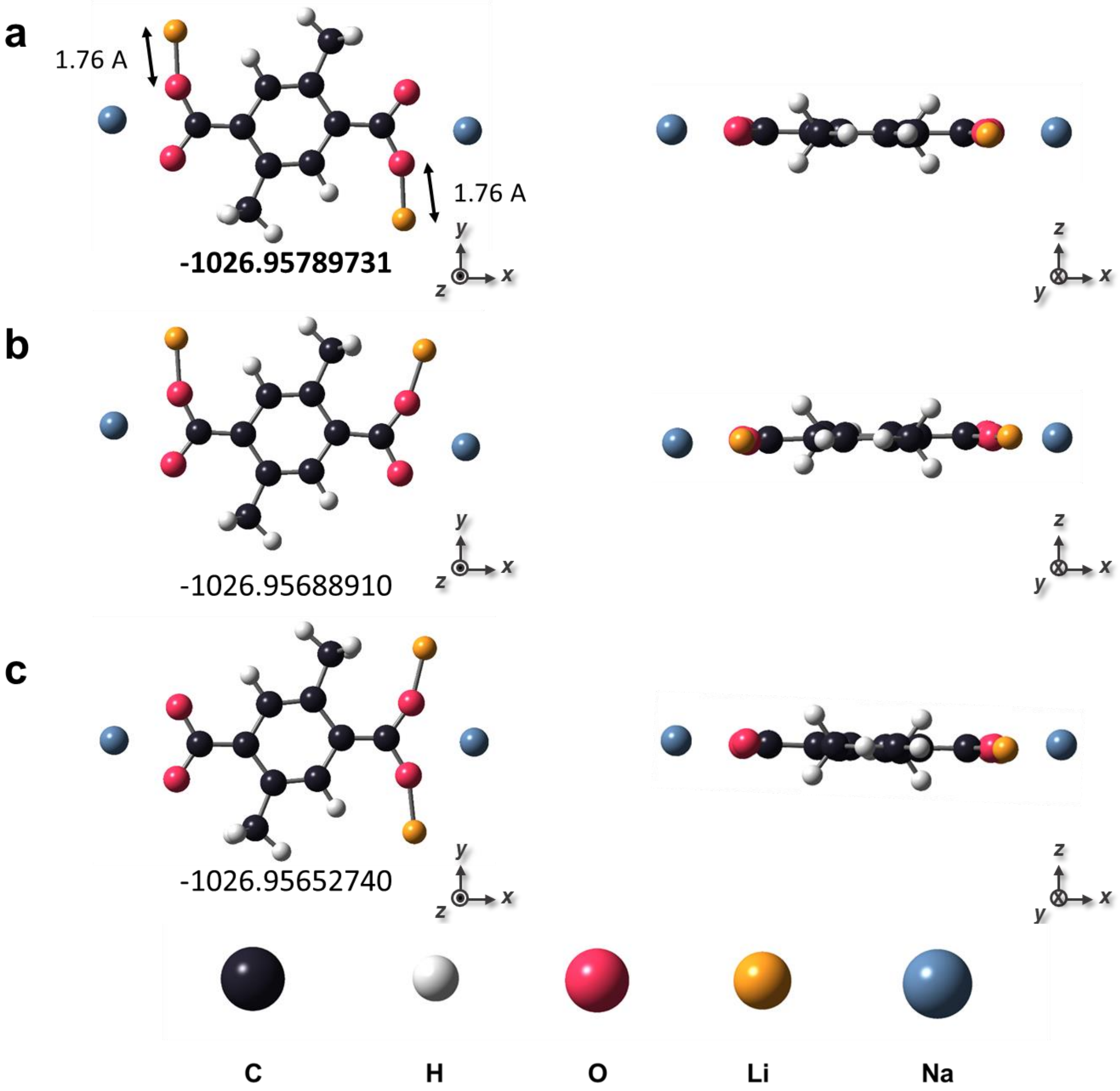

Figure S12 | Optimized geometries and total energy (in hartrees) of Na_2DMTP in solvated state after lithiation. (**a**) The most stable geometry and (**b**, **c**) different geometries of di-lithiated Na_2DMTP**.** Top views and side views are represented in the left and right panels along the Cartesian axes, respectively.

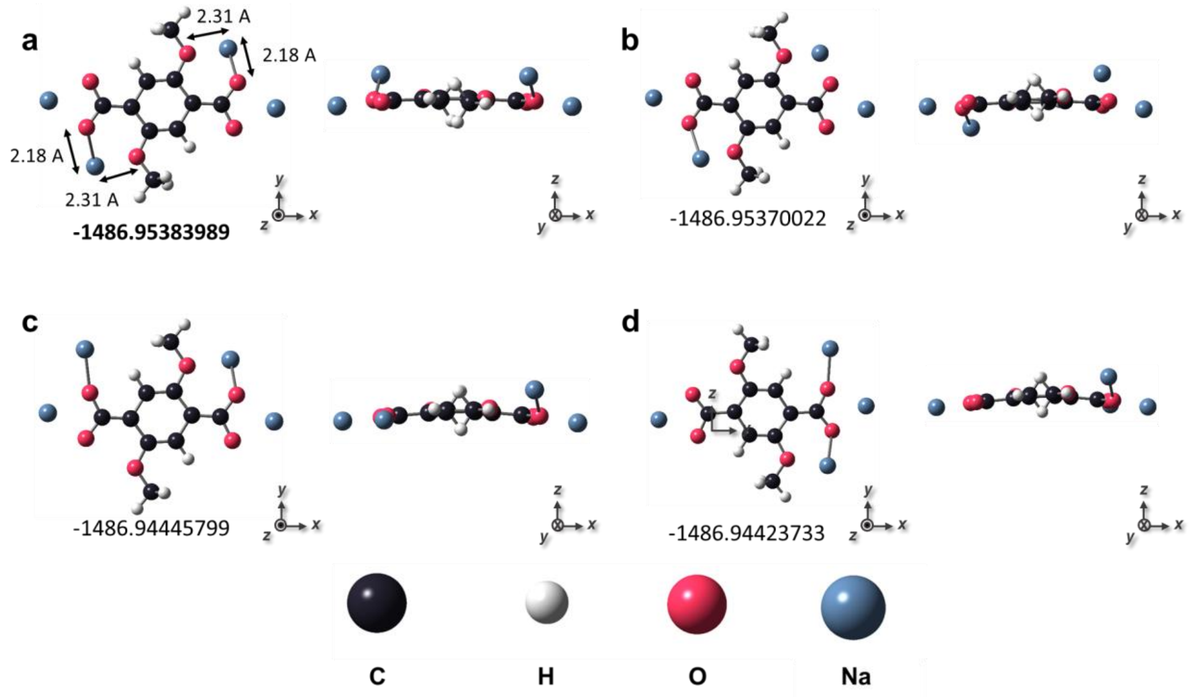

Figure S13 | Optimized geometries and total energy (in hartrees) of Na_2MeO_2TP in solvated state after sodiation. (**a**) The most stable geometry and (**b**–**d**) different geometries of di-sodiated Na_2MeO_2TP**.** Top views and side views are represented in the left and right panels along the Cartesian axes, respectively.

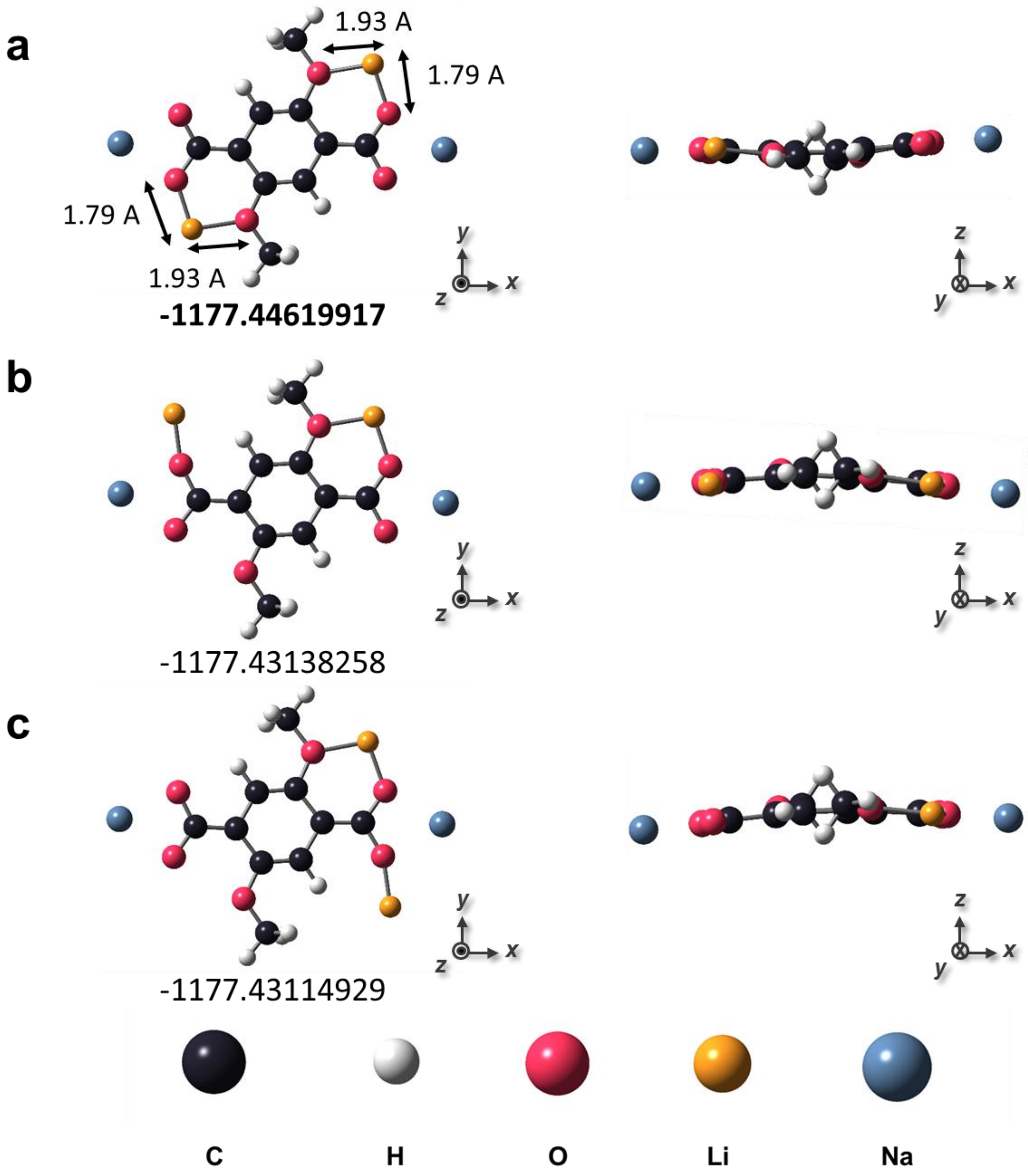

Figure S14 | Optimized geometries and total energy (in hartrees) of Na_2MeO_2TP in solvated state after lithiation. (**a**) The most stable geometry and (**b**, **c**) different geometries of di-lithiated Na_2MeO_2TP**.** Top views and side views are represented in the left and right panels along the Cartesian axes, respectively.